Energy & Environmental Science

High-Performance Carbon Nanotube Electronic Ratchets

Journal:	*Energy & Environmental Science*
Manuscript ID	EE-ART-07-2021-002048
Article Type:	Paper
Date Submitted by the Author:	03-Jul-2021
Complete List of Authors:	Hao, Ji; National Renewable Energy Laboratory, Chemistry & Nanoscience Center Nanayakkara, Sanjini; National Renewable Energy Laboratory, Material Science Tervo, Eric; National Renewable Energy Laboratory, Chemistry & Nanoscience Center Blackburn, Jeffrey; NREL, Ferguson, Andrew; National Renewable Energy Laboratory, Chemistry & Nanoscience Center

ARTICLE

High-Performance Carbon Nanotube Electronic Ratchets

Ji Hao,[a] Sanjini U. Nanayakkara,[b] Eric J. Tervo,[a] Jeffery L. Blackburn,[b] and Andrew J. Ferguson[a]*

Received 00th January 20xx,
Accepted 00th January 20xx

DOI: 10.1039/x0xx00000x

The rapid advancements in low-power portable/wearable electronic devices require concurrent development of technologies that can provide power without the need for bulky, heavy battery storage. Electronic ratchets, asymmetric transistor-based devices that can convert AC signals or electronic noise into DC power, have been proposed as one solution to this growing need. The recent demonstration of conjugated polymer-based electronic ratchets offers a route toward lightweight, flexible power sources for portable applications. Here we demonstrate the fabrication of the first electronic ratchets where the active channel component consists of semiconducting single-walled carbon nanotubes (s-SWNTs), which can transform electronic noise or AC signals to a stable DC current with higher output power (up to ca. 14 mW for a chemically doped device) than their polymer-based analogs. We also show that patterning of the dopant profile in the s-SWCNT channel enables reasonable power conversion performance (ca. 3.5 mW) with improved stability over the homogeneously doped devices. Our findings demonstrate the promise for s-SWCNT electronic ratchets as energy harvesting devices for portable, low-power applications.

Introduction

The increased interest in lightweight, flexible, portable/wearable electronic sensors and devices has spurred efforts to miniaturize components and create multifunctional devices. This has the potential to dramatically reduce their power consumption but also poses new challenges for the delivery of power to enable constant operation, potentially in remote locations. While existing battery technologies can sometimes provide a solution, they add to the weight/volume of the product, cannot guarantee uninterrupted power delivery over long periods of time, and introduce additional environmental and safety considerations. Several energy conversion technologies have been explored as alternatives for converting environmental energy into useful electrical power. These include conversion devices based on the thermoelectric,[1-5] pyroelectric,[6, 7] piezoelectric,[8, 9] and triboelectric[10] effects, as well as radio-frequency harvesters[11, 12] and, more recently, electronic ratchets.[13-21]

The electronic ratchet is a type of "Brownian Motor" where spatial or dynamical asymmetry can facilitate directed transport of charge carriers even in the presence of deterministic or random unbiased external input signals with a zero time-average amplitude.[21-23] The early examples of electronic ratchets were typically demonstrated in asymmetrically patterned architectures comprised of materials capable of supporting a two-dimensional electron gas (2DEG),[13-15, 24] often exhibiting superior performance at cryogenic temperatures. In 2011, Roeling et al. demonstrated the first "flashing" electronic ratchet based on a fairly simple organic field-effect transistor (OFET) architecture, where a time-dependent asymmetric potential is generated by applying periodic potentials to a pair of asymmetrically spaced interdigitated finger electrodes buried in the gate dielectric of the transistor.[16] More recently, flashing electronic ratchets have been demonstrated in GaAs nanowire devices patterned with multiple asymmetric Schottky gate electrodes,[17, 25] and in an OFET based on a polymer bulk-heterojunction with asymmetrically shaped finger electrodes buried in the gate dielectric.[19] In 2015, Mikhnenko et al. demonstrated a variation of the flashing ratchet device with a simplified OFET architecture,[18] where the asymmetry required to rectify the periodic or random input signal applied to the gate electrode was provided by a spatial variation in the counterion/charge distribution within a chemically-doped conjugated polymer exposed to a voltage stress.[18, 26] This simple architecture was subsequently employed for an electronic ratchet comprised of an n-type doped fullerene derivative,[27] modified to exploit the asymmetry provided by source and drain contacts fabricated from metals with different work functions,[28] and even prepared on a FET substrate fabricated from Al foil, Scotch tape, and graphite contacts.[29] Despite these recent demonstrations, the limited charge-carrier transport in disordered organic semiconductors[30] and properties related to the device architecture appear to restrict the performance of previously published organic electronic ratchets.[26]

Here we circumvent some of these limitations by replacing the disordered molecular or polymeric semiconductor with a network of enriched semiconducting single-walled carbon nanotubes (s-SWCNT). This material system offers several advantages over the more traditional organic electronic counterparts, since the extended pi electron network, inherent

[a] Chemistry and Nanoscience Center, National Renewable Energy Laboratory, Golden, CO 80401, USA
[b] Materials Science Center, National Renewable Energy Laboratory, Golden, CO 80401, USA
† Electronic Supplementary Information (ESI) available:
See DOI: 10.1039/x0xx00000x

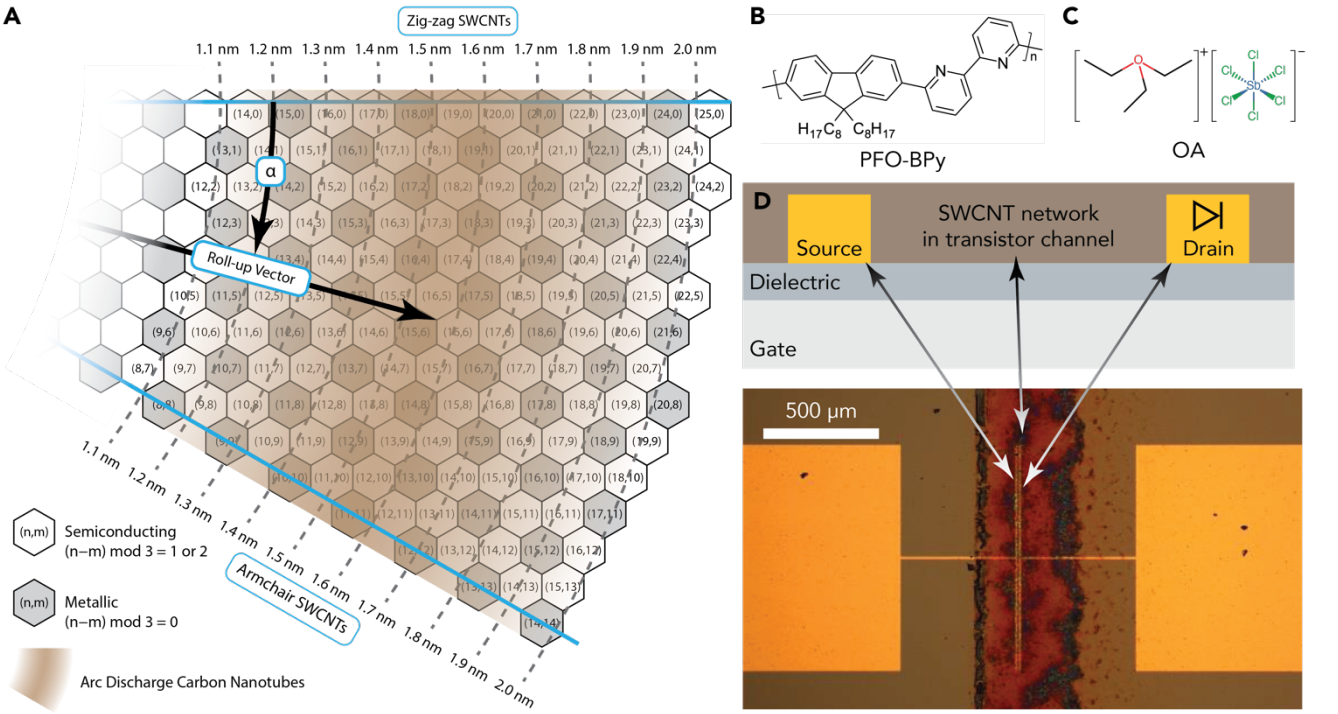

Fig. 1 Enriched Semiconducting Carbon Nanotube Field-effect Transistors. (A) Chirality map illustrating the diameter distribution of the SWCNTs present in the raw soot synthesized by the arc discharge method, where the SWCNT chirality is determined by the (n,m) indices that defines the roll-up vector and chiral angle, α. Determination of diameter distribution present in the samples studied here is detailed in Figure S1. (B) Polymer, PFO-BPy, used to selectively extract semiconducting carbon nanotubes (white hexagons in A) and (C) one-electron oxidant, OA, employed to *p*-type dope enriched s-SWCNT networks. (D) Schematic and optical microscope image of a carbon nanotube electronic ratchet device based on a field-effect transistor architecture. Nanotube Field-effect Transistors (A) Schematic and optical microscope image of a carbon nanotube electronic ratchet device based on a field-effect transistor architecture. (B) Chirality map illustrating the diameter distribution of the SWCNTs present in the raw soot synthesized by the plasma torch method. (C) Polymer, PFO-BPy, used to selectively extract semiconducting carbon nanotubes (white hexagons in B) and one-electron oxidant, OA, employed to p-type dope enriched s-SWCNT networks.

rigidity,[31] and low reorganization energy[32] of s-SWCNTs result in efficient intra- and inter-tube charge-transport that has enabled high-performance transistors to be fabricated with high charge-carrier mobilities.[33-36] Additionally, these properties, along with the rigid, porous network morphology, allow chemical doping processes to achieve very high electrical conductivities without disrupting the charge-carrier transport pathways.[37] We demonstrate that s-SWCNT-based electronic ratchet devices can be fabricated with a spatial asymmetry that is provided either by (i) a voltage bias that alters the counterion/charge-carrier distribution within the FET channel or (ii) pre-patterning the channel prior to doping. We show that in both cases, the devices can convert both deterministic and random input signals with zero time-averaged amplitude into DC current, and that the performance metrics of the devices are improved over prior organic electronic ratchets, with up to a 100-fold increase in the maximum output power (to ca. 15 mW). In devices that are homogeneously doped and then voltage stressed, scanning Kelvin probe force microscopy (KPFM) measurements indicate that asymmetric surface potentials result from the voltage stress, similar to observations for polymer-based ionic-organic ratchets,[18, 26, 38] suggesting a similar charge-pump mechanism for ratchet operation. Measurements probing the time dependence of the ratchet output indicate that the output current decreases over the course of several days for the voltage-stressed device, whereas the device doped after pre-patterning of the channel retains >95% of the initial current after 5 days.

Results and discussion

Basic ratchet device performance

Extraction of the semiconducting species from a raw soot of carbon nanotubes synthesized by the arc discharge method (shown schematically in the chirality map in Figure 1A) by the selective polymer poly[(9,9-dioctylfluorenyl-2,7-diyl)-*alt*-*co*-(6,6'-{2,2'-bipyridine})], PFO-BPy (Figure 1B), results in enriched inks of s-SWCNTs spanning the diameter range ca. 1.15 nm to 1.95 nm. See the supplementary information document for analysis of the absorbance spectra of these inks to extract the diameter distribution. We employ enriched arc discharge s-SWCNTs since they have been used in high-performance thin-film s-SWCNT network FETs[39, 40] or short-channel FETs with aligned s-SWCNTs,[33] where the charge-carrier transport in the latter is quasi-ballistic and the performance is comparable to silicon FETs. Field-effect transistors (FETs) of enriched arc discharge s-SWCNT networks (Figure 1D and Figure S3) were fabricated *via* spray deposition of these inks. The as-deposited 'undoped' s-SWCNT transistors are not intentionally doped with redox molecules but are likely (lightly) p-type, presumably by adventitious adsorption of oxygen or water molecules onto the surface of the nanotubes. 'Doped' s-SWCNT transistors are intentionally and homogeneously doped *p*-type with the one-electron oxidant triethyloxonium hexachloroantimonate, OA (Figure 1C), as shown by optical absorption (Figure S2) and FET transfer curves (Figure S4). Finally, pre-patterned s-SWCNT transistors are doped with OA on only one half of the channel,

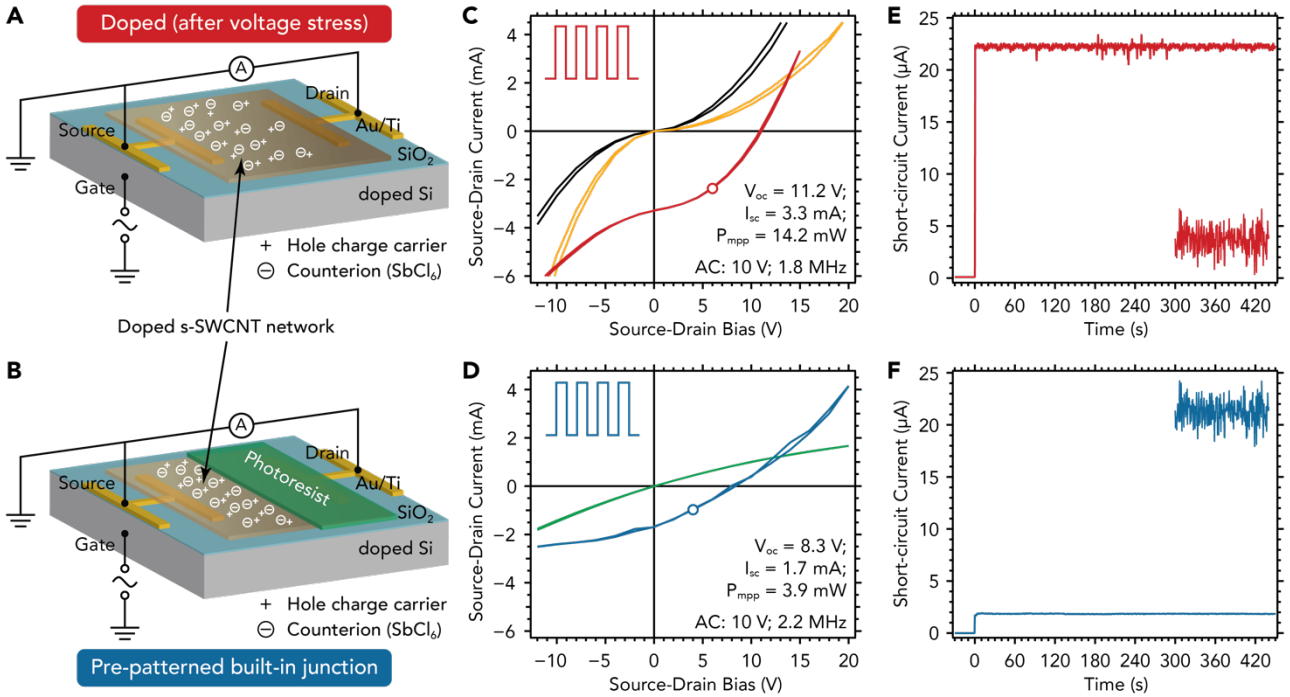

Fig. 2 Asymmetric Carbon Nanotube Electronic Ratchet Devices. Schematic illustrations of (A) an intentionally doped carbon nanotube ratchet device after voltage stress and (B) a pre-patterned carbon nanotube electronic ratchet with a built-in junction. Two-terminal current-voltage curves for (C) an intentionally doped (25 pg mL^{-1}) carbon nanotube ratchet device prior to (black curves) and after (yellow curves) voltage stress, and under application of a square wave signal applied to the gate electrode (red curves) and (D) the pre-patterned carbon nanotube electronic ratchet (green curves) and under application of a square wave signal applied to the gate electrode (blue curves). Short-circuit current output under application of a simulated electrical noise signal applied to the gate electrode for the (E) intentionally doped and (F) pre-patterned carbon nanotube electronic ratchets.

which creates a homojunction (p/p$^+$) in the center of the channel, so these devices are labeled 'built-in junction'. Schematics of each of the devices are shown in Figure 2 and Figure S5.

In the following discussion, we focus primarily on devices formed from enriched s-SWCNT networks doped intentionally with 25 pg mL^{-1} OA, since these are more amenable to characterization of the channel asymmetry (*vide infra*). In the case of the undoped device, the voltage stress applied to the drain electrode, V_D = −15 V for 10 minutes, results in non-linear current-voltage behavior (Figure S6A), indicative of a spatial asymmetry within the FET channel. In contrast, the enriched s-SWCNT network doped intentionally with OA already exhibits non-linear current-voltage behavior (Figure 2C), in this case resulting from the formation of a barrier to carrier injection into the channel from the contacts due to the presence of a background hole density from the doping process. In this case the voltage stress applied to the drain electrode, V_D = −15 V for 10 minutes, results in strong asymmetry in the current-voltage behavior, suggesting that the charge carrier/dopant counterion distribution within the channel is distorted by the applied bias. Similar to observations for ionic-organic electronic ratchets,[18] we suggest that the voltage stress causes a redistribution of the chemically-injected carriers and/or dopant counterions that modify the barrier at both contacts (see Kelvin probe force microscopy; *vide infra*), resulting in the observed rectifying behavior of the device. In the device where the semiconductor channel has been pre-patterned to restrict the doping to the drain contact side of the channel, the inherent doping asymmetry means that no voltage stress is required to yield similar non-linear current-voltage behavior (Figure 2D).

In all device configurations, the application of an unbiased radio-frequency (100 kHz – 10 MHz) AC square waveform to the gate electrode, results in rectifying behavior and a shift of the current-voltage curve to the power-generating fourth quadrant (Figures 2C-D and Figure S6A). With regards to the different ratchet configurations, devices that undergo voltage bias stressing exhibit a larger short-circuit current and improved power conversion than the pre-patterned, built-in junction device (c.f., Figures 2 and 3). The ratchet device that was intentionally *p*-type doped using a 5 pg mL^{-1} solution of OA produced the largest peak power output, whereas the device doped using a 25 pg mL^{-1} solution of OA exhibits the highest short-circuit current. For s-SWCNT devices doped using higher concentrations of OA, the device performance appears to be unstable, suggesting that the optimum performance is achieved for devices doped using OA solutions with concentrations lying in the range 5 – 25 pg mL^{-1}. We note here with caution that this observation may not be universal for all enriched s-SWCNT/polymer combinations and my depend on the exact nature of the SWCNT starting material and the polymer employed for selective extraction of the semiconducting species. Although it is difficult to estimate the charge-carrier doping level for chemically-doped s-SWCNT networks, particularly those comprised of multiple carbon nanotube chiral species, the extent of absorbance bleaching observed (Figure S2) suggests a moderate doping level in the samples studied here. We therefore attribute the improved device performance to enhanced electrical conductivity (c.f., charge-carrier mobility

in Figure 3 and Figure S4) and rectification behavior. As with the studies previously published for ionic-organic ratchets, the high impedance of our s-SWCNT transistor devices means that we are operating under 'impedance bridging' conditions.[18] Under these conditions, the voltage amplitude sourced by the pulse/function generator and applied to the gate electrode of the ratchet architecture is double the nominal voltage setting (e.g., for a nominal zero-to-peak voltage amplitude, V_n, setting of 5 V the actual voltage amplitude, V_a, is 10 V).

Application of an alternating current (AC) waveform (square-wave) to the gate electrode (V_a = 10 V, f = 1.8 MHz) of the 25 pg mL^{-1} OA-doped device results in a I_{sc} of 3.3 mA (Figure 2C), almost double that of the undoped and pre-patterned devices, and a P_{max} of ca. 14.2 mW. While the performance of the pre-patterned ratchet device is not as impressive as the voltage stressed devices, reasonable rectification behavior is still observed, and the device yields a I_{sc} of 1.7 mA – more than two orders of magnitude larger than a previously reported non-voltage stressed organic ratchet[28] – and a P_{max} of ca. 3.9 mW (Figures 2D). Like polymer-based ionic-organic ratchet devices, these carbon nanotube devices can also function as energy harvesting devices for simulated electrical noise signals, exhibiting short-circuit currents, I_{sc}, on the order of a few µA to a few tens of µA (Figures 2E-F). The improved current generation for the voltage-stressed ratchet can also be seen under the application of simulated electronic noise to the gate electrode, where the intentionally *p*-type doped ratchet produces a I_{sc} of >20 µA.

Under application of an unbiased alternating voltage signal (either an AC square wave or simulated noise) to the gate electrode, during periods with a negative bias holes are primarily injected from the source electrode, 'charging' the ratchet device. In contrast, during periods with a positive bias, holes can be extracted from either contact. However, since holes are primarily injected from the source the alternating voltage signal to the gate results in net current flow from source to drain.

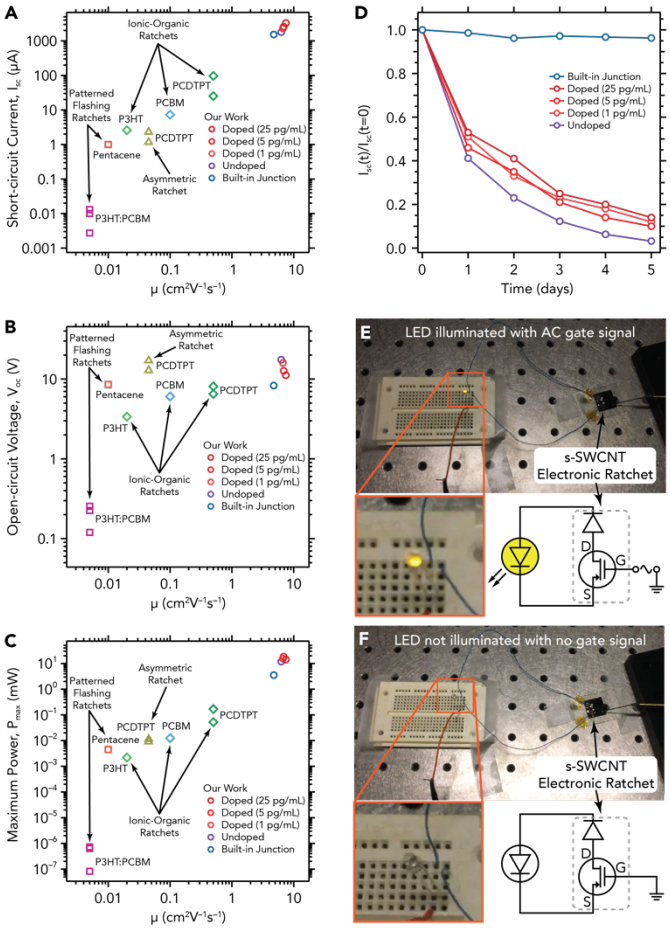

Fig. 3 Performance, Stability, and Application of Carbon Nanotube Electronic Ratchet Devices. (A) Short-circuit current, I_{sc}, (B) open-circuit voltage, V_{oc}, and (C) maximum power, P_{max}, as a function of the charge-carrier mobility, µ, of electronic ratchets comprised of various organic semiconductor systems. Note: the amplitude for the periodic AC bias, V_a, applied to the gate electrode is 10 V for the s-SWCNT electronic ratchets in this work and 10 V for most of the electronic ratchets in the literature. (D) The time-dependence of I_{sc} for the various s-SWCNT electronic ratchet devices prepared in this work. (E, F) Digital photographs illustrating that application of a square wave AC bias (V_a=10 V, f=2.2 MHz) to the gate electrode of the pristine undoped s-SWCNT electronic ratchet device is sufficient to power a light-emitting diode.

Comparisons to published organic electronic ratchets

Since the pioneering work on ionic-organic flashing ratchets based on polymers inspired this exploration of carbon nanotube ratchets, it is informative to make some direct comparisons to previously published organic electronic ratchet devices (Figures 3A-C). It should be noted here that the data is extracted from the publications for these organic electronic ratchets for the experimental conditions that are reported to yield the optimum device performance,[16, 18, 19, 26-28] while also trying to select data where the experimental conditions are as similar as possible for more convenient and direct comparison. We have not made any effort to reproduce this literature data.

In all cases, the current (Figure 3A) and power (Figure 3C) generated by the carbon nanotube ratchet devices exceed those previously reported for electronic ratchet devices based on polymeric and molecular organic semiconductors. In the case of I_{sc} and P_{max}, the device parameters appear to scale roughly linearly with the charge carrier mobility for the semiconductor employed in the transistor channel (c.f., Figure S7 for the dependence of I_{sc} on the charge-carrier mobility for the s-SWCNT electronic ratchets). This observation provides justification for the choice of semiconducting carbon nanotubes for electronic ratchets, since they have the potential for high charge carrier mobilities even in thin-film networks of randomly aligned SWCNTs, but also points toward high-mobility semiconducting conjugated polymers as potential alternatives. In contrast, the open-circuit voltages, V_{oc}, of organic electronic ratchets has a much weaker dependence on the charge carrier mobility and the V_{oc} of carbon nanotube ratchet devices are similar to those for most electronic ratchets based on polymers and molecular semiconductors (Figure 3B). Figure S8 also illustrates that the device short-circuit current output scales with the amplitude of the applied bias.

Ratchet device performance stability and utility

The demonstration of power generation from unbiased periodic or random signals is exciting, but an underexplored metric for electronic ratchets is the stability of the device output.

Figure 3D illustrates the device stability for the three device configurations, including voltage stressed devices that were previously homogeneously doped with three different doping levels (OA concentrations: 1 pg mL^{-1}, 5 pg mL^{-1}, 25 pg mL^{-1}). While the initial device performance of the pre-patterned device is lower than that of the voltage stressed devices, >95% of the I_{sc} is retained for repeated measurements over 5 days, whereas the voltage stressed devices lose >85% of the I_{sc} over the same period. Figure S9 in the supplementary materials illustrates that all of our doped s-SWCNT ratchets exhibit slightly better device performance stability (short-circuit current output) than polymer-based ionic-organic ratchets published previously.[28] The reduction in device performance is likely due to a slow redistribution of the dopant counterions and/or charge carriers in the absence of a source-drain bias, as shown for chemically-doped conjugated polymers,[38] or potentially due to an instability in the chemical doping within an unprotected transistor channel. It is interesting to note that the device with the pre-patterned built-in junction retains a large fraction of the initial I_{sc}. While we do not have direct experimental evidence to confirm the origin of this improved stability, it is possible that the photoresist polymer that remains on one portion of the device (Figure 2B) prevents dopant counterion redistribution throughout the channel. Although none of the s-SWCNT devices exhibit an 'activation' of the device performance, as observed for polymer-based ratchets with source and drain contacts fabricated from metals with different work functions,[28] the short-circuit current is still superior to previously published ionic-organic ratchets even after 5 days degradation in performance.

Although the power generated by a single electronic ratchet is low (<15 mW), even the 'undoped' electronic ratchet generates sufficient power to illuminate a low-power light-emitting diode, LED, (Figures 3E) when driven by a square wave AC signal (V_a=10 V, f=1.8 – 2.2 MHz). Figure 3F shows that the LED remains unlit when no signal is applied to the gate electrode. Although the applied voltage signal, and the resulting device output, is not optimized to drive the LED at its full brightness, this is still a clear demonstration that electronic ratchets hold promise for low-power portable electronic applications, particularly when built into larger, multi-device energy harvesting systems. A video showing the electronic ratchet-driven LED is provided in the Supplementary Materials.

Frequency-dependent ratchet device performance

To further explore the performance of the s-SWCNT electronic ratchet devices, we measure the dependence of the device parameters (I_{sc}, V_{oc}, and P_{max}) on the frequency of the applied square wave AC signal (V_a=10 V, Figure 4). All three device parameters increase dramatically as the frequency is increased from 100 kHz to ca. 2 MHz, exhibiting qualitative similarities to previously reported ionic-organic ratchets.[18, 26]

Mikhnenko et al. pointed out that the net short-circuit current (units: A), I_{sc}, for an electronic ratchet operating as a charge pump at low frequencies can be described by:

$$I_{sc} = 2\eta f C V_a \quad (1)$$

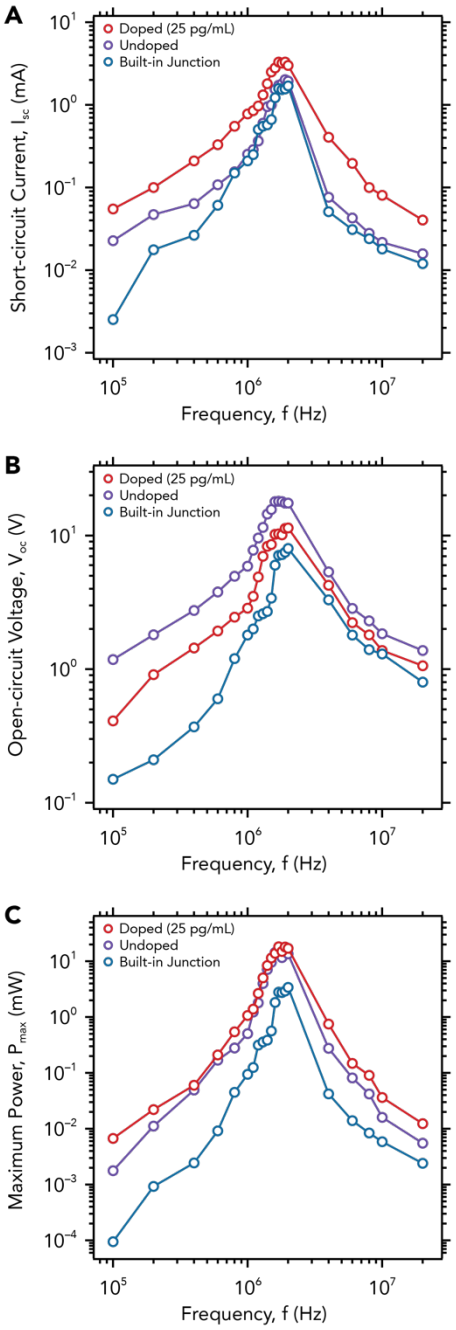

Fig. 7 Frequency-dependent Performance of Carbon Nanotube Electronic Ratchet Devices. Variation in the (A) short-circuit current, I_{sc}, (B) open-circuit voltage, V_{oc}, and (C) maximum power, P_{max}, as a function of frequency, f, of the periodic, square wave AC bias applied to the gate electrode (V_a=10 V).

where f and V_a are the frequency (units: Hz or s^{-1}) and amplitude (units: V) of AC oscillation, respectively, C is the gate-channel capacitance (units: F or A s V^{-1}), and η is the charge displacement efficiency (i.e., fraction of the total charge collected at the drain electrode). At frequencies below ca. 500 kHz the s-SWCNT electronic ratchet devices described here appear to follow this linear dependence on frequency, suggesting that the channel capacitor can be fully charged and discharged during the waveform period. However, at higher frequencies the dependence becomes more pronounced, suggesting that the gate-channel capacitance and charge

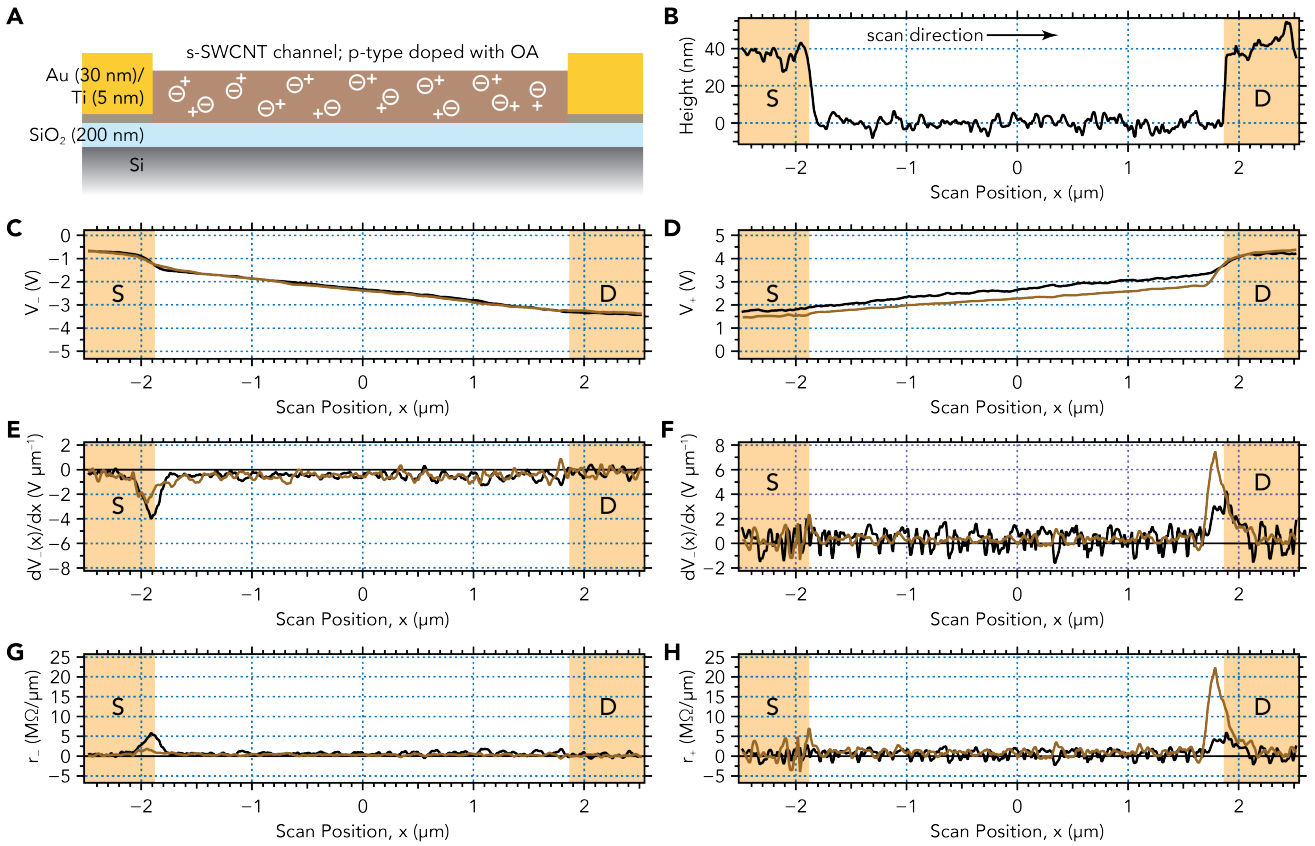

Fig. 8 Surface Potential Profiles of Homogeneously Doped Carbon Nanotube Ratchet. (A) Schematic and (B) topography of the transistor channel, illustrating the scan direction used for extraction of the line profiles. (C, D) Surface potential, (E, F) differential potential (i.e., field), and (G, H) differential resistance measured under application of a drain bias of (C, E, G) V_D = −5 V or (D, F, H) V_D = +5 V. Black traces correspond to the as-prepared device, whereas brown traces correspond to the device after application of a voltage stress (V_D = −15 V for 10 minutes) to induce asymmetry.

displacement efficiency may also exhibit frequency-dependent behavior. Above the frequency for peak power output, f_{peak} (ca. 2 MHz), the channel capacitor cannot be fully charged and discharged during the waveform period, resulting in a reduction of the I_{sc} and P_{max} with increasing frequency.

The behavior observed here is qualitatively similar to that for both ionic-organic electronic ratchets[18, 26, 27] and polymer electronic ratchets with asymmetric contacts,[28] where the device performance metrics improve with increasing frequency of the signal applied to the gate electrode of the transistor device. As observed for both ionic-electronic ratchets employing poly(3-hexylthiophene-2,5-diyl), P3HT, or phenyl-C_{61} butyric acid methyl ester, PCBM, as the active channel material, the device metrics reach a peak at a specific drive frequency of the signal applied to the gate electrode.[18, 27] This behavior corresponds to a maximum frequency (ca. 2 MHz) at which the ratchet can be fully charged-discharged during the waveform period, and suggests that the devices presented here exhibit a response time on the order of 72 ns to 94 ns. Improvements in the material properties and/or modification of the device architecture are likely to facilitate electronic ratchets that can operate efficiently at higher frequencies.

Probing the electronic ratchet asymmetry

In order to understand the observed rectifying behavior of the homogeneously doped ratchet device, we employed Kelvin probe force microscopy (KPFM) to measure the surface potential profile (units: V), V(x) (Figure 5). KPFM has been used to explore electrochemical doping, injection barriers, and rectifying junctions in organic transistor-based devices such as light-emitting electrochemical cells, [41, 42] field-effect transistors,[43-46] and organic-ionic ratchets.[18] Prior to voltage stressing, the electronic ratchet homogeneously p-type doped with a 25 pg mL^{-1} solution of OA exhibits a potential drop related to the hole-injecting contact: the source electrode when V_D = −5 V (Figure 5C) or the drain electrode when V_D = +5 V (Figure 5D). The potential drop can be attributed to a differential resistance (units: Ω m^{-1}) (barrier), r(x), calculated according to:

$$r(x) = \frac{d}{dx}R(x) = \frac{1}{I_{SD}}\frac{d}{dx}V(x) \qquad (2)$$

where R(x) is the resistance (units: Ω) of the portion of the device between the source electrode and the position x; V(x) is the surface potential profile (units: V) at position x; and I_{SD} is the current (units: A) flowing through the device when a voltage, V_D, is applied to the drain electrode. For the as-prepared device, the differential resistance exhibits identical peaks at both the source and drain contacts (Figures 5G-H), as would be expected for a spatially symmetric device and corresponding to a contact resistance (barrier) of ca. 5 MΩ μm^{-1}.

After voltage stressing the potential drop increases at the drain electrode and is reduced at the source electrode

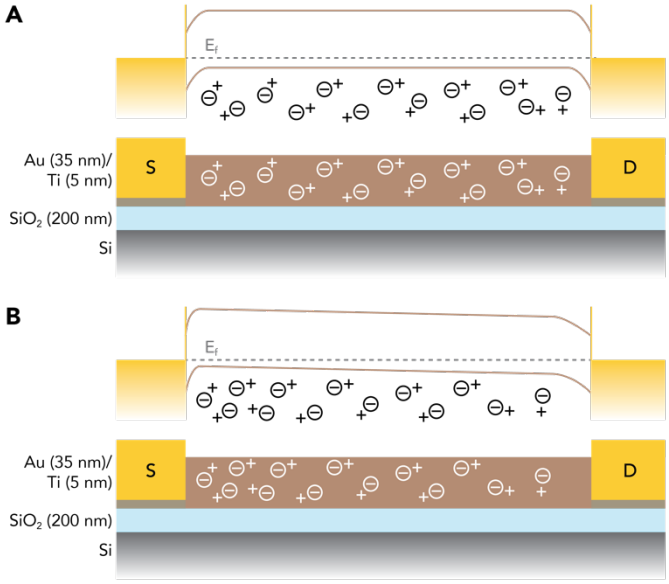

Fig. 9 Contact Barriers in Doped and Voltage Stressed Carbon Nanotube Ratchets. Schematic cartoon illustrating the charge carrier/dopant counterion distributions in the (A) as-prepared homogeneously doped carbon nanotube electronic ratchet and (B) the same device after application of a voltage stress (V_D = −15 V for 10 minutes). The cartoon illustrates that the symmetrical barriers (height and width) to hole injection are decreased at the source (S) contact and increased at the drain (D) contact, as a result of the biased-induced redistribution of the charged species within the transistor channel.

(Figures 5C-D), resulting in asymmetric differential resistances for the two contacts (Figures 5G-H). This suggests that the contact resistances have been altered as a result of the biasing process, an observation that could be attributed to the redistribution of charge carriers and/or dopant counterions.[47-49] Under application of a bias of >5 V, positive charge carriers (holes), injected either through the chemical doping process or via injection from the contact, would transit the device in less than 30 ns (assuming a reasonable hole mobility of ca. 1 $cm^2 V^{-1} s^{-1}$). We therefore posit that the –15 V bias applied during the stressing process drives the dopant counterions from their equilibrium (as-deposited) position, with depletion of the counterions close to the drain contact and their accumulation close to the source contact. Upon removal of the bias potential, holes quickly redistribute because of the field induced by the asymmetric counterion distribution. This results in a change in the local carrier density along the channel, which is known to have a strong impact on the properties of a Schottky barrier between an organic semiconductor and metal contact[47-49] and the electric field distribution throughout the device.[41, 46] The depletion of counterions and holes close to the drain contact increases the contact resistance and associated barrier for hole injection (Figures 5H), whereas their accumulation at the source contact interface decreases the barrier for hole injection (Figures 5G).[48]

These changes in the charge carrier/dopant counterion distribution, and the impacts this redistribution would have on the barrier properties (height and width), due to the voltage stress is shown schematically in Figure 6. In contrast to the electrode-dependent carrier *injection* barriers, there appears to be no significant barrier for hole *extraction* at either contact. This suggests that holes will be predominantly injected at the source and extracted from either contact, during negative or positive potential swings at the gate electrode, respectively. This is consistent with the formation of a rectifying contact at the drain electrode and helps to rationalize the observed current-voltage response. Similar behavior is qualitatively consistent with that observed for an electronic ratchet based on the semiconducting polymer poly(3-hexylthiophene-2,5-diyl) (P3HT) *p*-type doped using trityl tetrakis(pentafluorophenyl)borate (TrTPFB).[18]

For the pre-patterned device, the s-SWCNT channel is covered by a 1.8-µm thick photoresist layer, which is masked to allow photolithographic exposure of one end of the channel and subsequent removal of the exposed photoresist. The remaining photoresist layer provides protection to the underlying s-SWCNT network during the solution-phase doping process (soaking in OA solution for 1 min at 78 °C).[50] Unfortunately, this same photoresist layer prevents KPFM from probing the potential distribution across the channel. Since the photoresist is transparent to infrared wavelengths, we turn to scanning confocal Raman microscopy for excitation at 785 nm as a method to probe the doping distribution that results from the patterning process. In Figure 7A we show the impact of *p*-type doping on the Raman spectrum, illustrating a decrease in the intensity of the G' mode relative to the G^+ mode, which provides a metric for probing the injected carrier density into the s-SWCNT network. We find that the relative intensity of the G' and G^+ modes are the most sensitive to charge carrier doping, at least for the dopant concentration employed in this work. Figure 7B shows a schematic of the scanning confocal Raman microscopy experimental setup and the corresponding Raman mapping results are plotted in Figures 7C-D.

For an undoped s-SWCNT network, the G':G^+ intensity ratio is >0.6, and this ratio drops with increasing p-type doping to a value around 0.35 for a s-SWCNT network doped by an OA solution with a concentration of 25 pg mL (Figure 7A). The Raman mapping data illustrate that the photoresist provides protection to the underlying s-SWCNT network, preventing the OA dopant from accessing the s-SWCNT surface and doping the carbon nanotubes (G':G^+ intensity ratio is >0.6; Figure 7D). In the region of the device exposed to the OA dopant the G':G^+ intensity ratio is ca. 0.4, indicating that the s-SWCNTs are *p*-type doped. The protected region of the nanotube network is slightly *p*-type due to adventitious doping from either O_2 of H_2O adsorbed onto the network surface prior to, or because of, the photoresist deposition process. As a result, a p^+/p junction is formed in the middle of the transistor channel, which provides a rectifying junction that results in the net flow of holes from source to drain (c.f., Figure 2B). The data in Figure 7D also suggest that the simple patterning process developed here can produce junctions that are quite narrow (<1 µm; with the resolution limited by the spot size in our measurements) and could be employed to generate rectifying junctions in other materials, such as conjugated polymers, inorganic, and hybrid semiconductors.

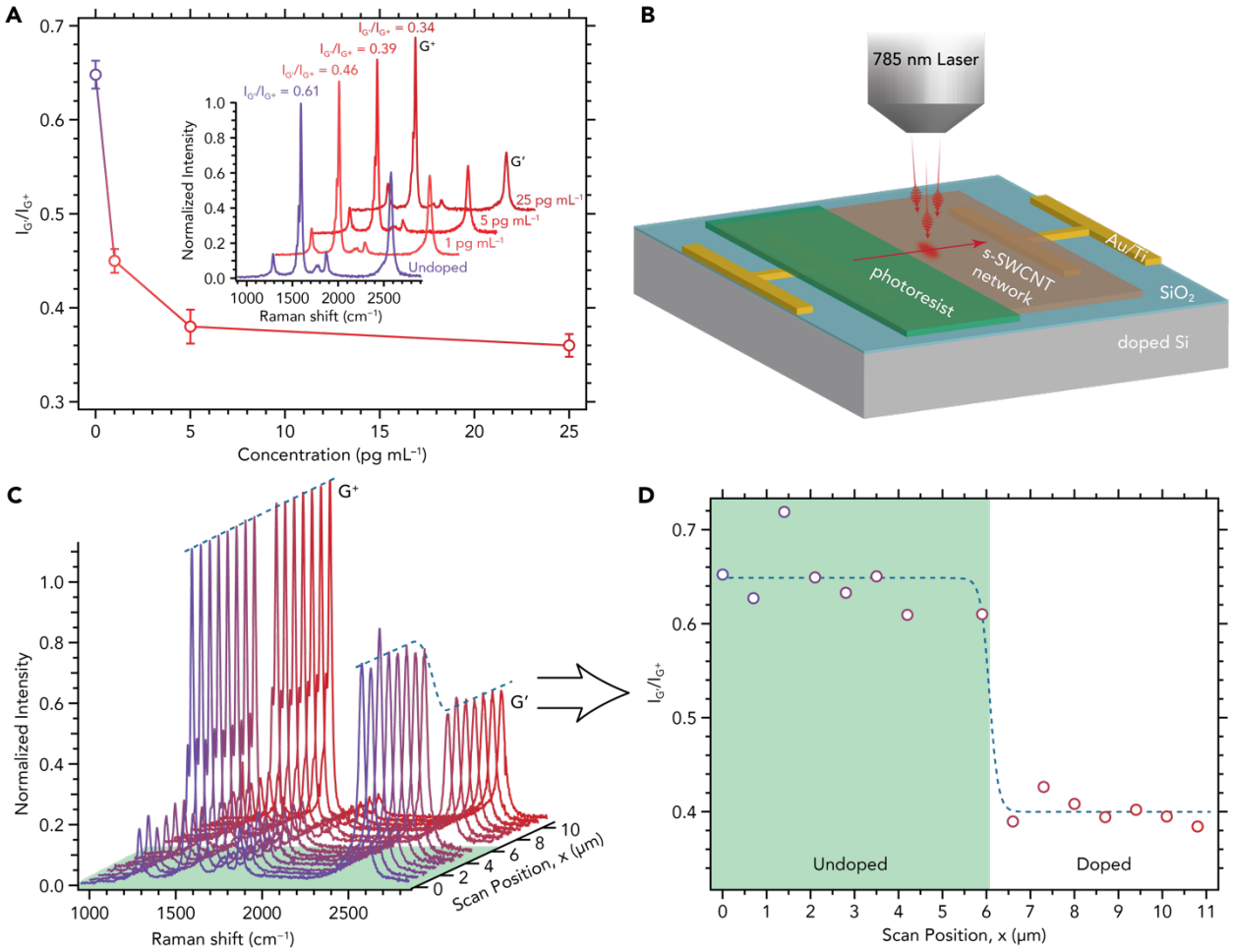

Fig. 10 Characterization of Pre-patterned Carbon Nanotube Ratchets. (A) Intensity ratio of the G' and G⁺ modes as a function of concentration of the p-type dopant employed in the solution doping step. The inset shows representative Raman spectra for the different doping concentrations. (B) A schematic depicting the Raman mapping experiment of the pre-patterned, doped carbon nanotube electronic ratchet. (C) Raman spectra and (D) Intensity ratio of the G' and G⁺ modes as a function of scan position along the channel, showing a clear transition between doped and undoped regions.

Conclusions

In summary, we demonstrate that p-type doped networks of enriched s-SWCNTs represent an excellent candidate as the active material for transistor-based electronic flashing ratchets. These devices are capable of rectifying simulated electronic noise and periodic AC signals with a zero time-average amplitude applied to the transistor gate electrode. Under application of a square waveform AC signal with an amplitude of 10 V the devices produce >1 mA short-circuit current and peak output power >10 mW, capable of driving simple lower-power electronic components, such as an LED. Our carbon nanotube-based electronic ratchets surpass the performance of previously published electronic ratchets that employ doped conjugated polymers. We demonstrate that a simple voltage biasing process can redistribute the dopant counterions and positive charge carriers, altering the Schottky barriers at the transistor contacts and creating a spatial asymmetry in the transistor channel that facilitates the observed rectifying behavior. We also develop a simple patterning process that enables the formation of a rectifying junction in the middle of the channel, illustrating that the rectifying behavior does not necessarily need to be associated with the barriers formed at the interface between the contact and semiconductor channel. These results point to the potential for carbon nanotube electronic ratchets for remote and portable power generation and for further exploration into the material properties and device characteristics to understand and improve their energy conversion performance.

Experimental methods

Materials

The raw SWCNT material, synthesized *via* the arc-discharge (AD) method, was purchased from Sigma-Aldrich (SKU 698695; Lot#MKBC7933V). Poly[(9,9-dioctylfluorenyl-2,7-diyl)-*alt*-co-(6,6'-{2,2'-bipyridine})] (PFO-BPy), was used as received from American Dye Source (ADS153UV; Lot #161002A1; M_w = 55 kDa).

Preparation of polymer/s-SWCNT inks

The polymer solution (1–2 mg mL^{-1} in toluene with maximum volume of ca. 15 mL in a 20 mL borosilicate scintillation vial) is

agitated in a heated ultrasonic bath for several minutes to ensure full solvation of the polymer. Raw (unprocessed) SWCNT soot is mixed with the pre-prepared polymer solution at a concentration of 1–2 mg mL^{-1}. The polymer solution is added to the SWCNT powder, at a ratio determined to optimize the yield and selectivity for s-SWCNT extraction, and the mixture is then placed in an ultrasonic bath for at least 1 min. The nanotube/polymer mixture is then processed in the vial with a probe tip ultrasonic processor (Cole Parmer CPX-750, 1/2'' tip) for 30 min at 40% amplitude. During this process, the vial is typically submerged in flowing, cool water at ca. 18 °C).

Immediately following the ultrasonic process, the contents of the vial are transferred to a centrifuge tube and processed at 20 °C, 13,200 rpm, for 5 min (Beckman Coulter L-100 XP ultracentrifuge, SW-32 Ti rotor). The supernatant containing polymer-wrapped s-SWCNTs and excess polymer is collected *via* pipette. To minimize the concentration of excess polymer in solution, and to capture excess polymer for re-use, the dispersion supernatant is reprocessed, but at higher rotational force and reduced temperature, typically at 20 °C, 24,100 rpm, for 20 h. The resulting supernatant typically contains only unbound polymer in solution and can be collected for reuse, while the pellet contains polymer-wrapped s-SWCNTs with very little excess polymer. The s-SWCNT ink is then prepared by dispersing the pellet in neat toluene: typically, multiple pellets can be dispersed in one scintillation vial, depending on the desired concentration for subsequent processing. The pellet(s):toluene combination is then processed in a heated ultrasonic bath for 5 min or more to yield a homogeneous polymer:s-SWCNT ink. If necessary, this excess polymer removal process is repeated until the desired PFO-BPy:s-SWCNT ratio is obtained.

Preparation of s-SWCNT networks and electronic ratchet devices

The polymer:s-SWCNT ink is printed at a flow rate of 300 mL min^{-1}, directed by a stream of dry nitrogen gas at 7 std L min^{-1}, onto either clean glass or pre-patterned field-effect transistor (FET) substrates on a heated stage (130 ± 10 °C) using an ultrasonic spray head (Sonotek; 120 kHz; 0.8 W) equipped with an Impact spray shaping system with raster pattern designed to maximize uniformity over the sample area. After printing, excess polymer is removed from the s-SWCNT network by submersion in neat toluene for at least 10 min at 78 °C. The thin-film network is then dried under gentle nitrogen flow.

Electronic ratchet devices were fabricated onto pre-patterned FET substrates purchased from University Wafer (Product #3401), where the transistor contacts were composed of gold contact pads (ca. 30 nm of Au on a ca. 5 nm Ti wetting layer) via thermal evaporation through a photolithographically defined pattern onto a 200 nm silicon dioxide (SiO_2) gate dielectric on a highly doped silicon substrate (1–10 Ω cm). The standard FET architecture employed in this study consisted of channel lengths (L_{ch}) of ca. 4.0 ± 0.5 µm between 1000-µm wide gold source and drain electrodes. The highly doped silicon substrate was employed as the gate contact. Homogeneously p-type doped electronic ratchets were prepared by immersion of the device in a solution of triethyloxonium hexachloroantimonate (OA; Sigma-Aldrich) in dichloromethane at 78 °C for 1 min, followed by a short (<1 sec) dip in acetone to remove dopant residue. Samples in this study were doped with OA solutions with concentrations of 1 pg mL^{-1}, 5 pg mL^{-1}, and 25 pg mL^{-1}. The pre-patterned device was prepared by optical lithography of a device with a 25 µm channel coated with photoresist (Microchem S1818). Following removal of the developed photoresist, the device was immersed in a 25 pg mL^{-1} solution of OA in dichloromethane at 78 °C for 1 min.

Current-Voltage and Field-effect Transistor Measurements

The typical current-voltage (I-V) measurement (Figure 2C–D) was performed by using one Keithley 2400 source meter (controlled with a laptop running a custom LabVIEW program to perform the measurement and collect experimental data) connected to the source and drain contacts. Typical field-effect transistor measurements were performed by using two Keithley 2400 source meters (controlled with a laptop running a custom LabVIEW program to perform the measurement and collect experimental data). One Keithley 2400 source meter was used to supply the source-drain voltage and monitor the source-drain current and the other was used to supply the gate voltage and monitor the gate-channel current.

Electronic ratchet measurements

AC signals and electronic noise were supplied to the gate electrode of the electronic ratchet device by either an Agilent 33220A signal generator or Keysight 81150A Pulse Function Arbitrary Noise generator, respectively. The waveform of the AC signal and electronic noise signal were acquired by using Tektronix Oscilloscope TBS 1152B. Since the impedance of our s-SWCNT transistor devices significantly exceeds the output impedance (50 Ω) of our signal/function generator(s) this means our measurements are operating under 'impedance bridging' conditions. Therefore, the voltage amplitude sourced by the pulse/function generator and applied to the gate electrode of the ratchet architecture is double the nominal voltage setting (e.g., for a nominal zero-to-peak voltage amplitude, V_n, setting of 5 V the actual voltage amplitude, V_a, is 10 V). The source-drain current of the device was monitored by a Keithley 2400 source meter with Pi-filter inserted between the source meter and electrodes. The frequency dependence of the electronic ratchet device performance (I_{sc}, V_{oc}, P_{max}) was determined by either:

1. A full I-V sweep, where the source-drain current (I_{SD}) was measured while sweeping the source-drain bias (V_{SD}) following 0 V → +20 V → –20 V → 0 V while a 10 V amplitude square waveform AC signal with the chosen frequency (f) was applied to the gate electrode, or;
2. Measuring the short-circuit current (I_{sc}) at V_{SD} = 0 V and open-circuit voltage (V_{oc}) at I_{SD} = 0 mA independently while a 10 V amplitude square waveform AC signal with the chosen frequency (f) was applied to the gate electrode.

The yellow-green GaP LED (Purdy Electronics AND124G), with a 25 mA forward current and 2.1 V forward voltage, was purchased from Allied Electronics & Automation.

Atomic force and Kelvin probe force microscopy

The surface topography and contact potential difference of the electronic ratchet devices were measured in non-contact (tapping) mode on a Park Systems XE70 Atomic Force Microscope (AFM) using ElectriMulti75-G probes (Multi75E-G from Budget Sensors, Cr/Pt coated for electrical measurements). Topographic and potential images were measured simultaneously during the probe scanning, using a single-pass system. To remove measurement artifacts due to tilt between probe and sample planes, the raw topography images were flattened using the Park Systems XE70 Imaging software package. KPFM measures the contact potential difference between the probe and sample by nullifying the Coulomb forces experienced by the tip, which is due to the work-function difference between the probe and sample. KPFM measurements were performed with the source contact grounded and with either a V_{SD} bias of +5 V or −5 V of the FET. The source-drain bias (V_{SD}) was supplied by DC power supply (9312-PS, Marlin P. Jones & Associates Inc.).

Optical absorption and Raman scattering spectroscopy

Absorbance measurements were performed on an Agilent Cary 5000 spectrophotometer, with a step size of 2 nm and scanning speed of 600 nm min^{-1}. The blank substrate was calibrated as the baseline before the film measurement.

High-resolution Raman spectroscopy of pristine and doped s-SWCNT networks were performed in a confocal Raman microscope (Renishaw inVia RE04) system with a 100x objective lens, following excitation by a 785 nm (1.58 eV) laser. The software-controlled excitation intensity was set to 0.01%. Raman scattering was detected using a grating with 1800 lines mm^{-1} with 1 sec integration time for 8 accumulations.

Conflicts of interest

There are no conflicts to declare.

Acknowledgements

This work was authored by the National Renewable Energy Laboratory (NREL), operated by Alliance for Sustainable Energy, LLC, for the U.S. Department of Energy (DOE) under Contract No. DE-AC36-08GO28308. This work was supported by the Laboratory Directed Research and Development (LDRD) Program at NREL. The views expressed in the article do not necessarily represent the views of the DOE or the U.S. Government.

Notes and references

1. M. Orrill and S. LeBlanc, *J. Appl. Polym. Sci.*, 2017, **134**.
2. R. Kroon, J. D. Ryan, D. Kiefer, L. Yu, J. Hynynen, E. Olsson and C. Müller, *Adv. Funct. Mater.*, 2017, **27**, 1704183.
3. J. L. Blackburn, A. J. Ferguson, C. Cho and J. C. Grunlan, *Adv. Mater.*, 2018, **30**, 1704386.
4. K. Nan, S. D. Kang, K. Li, K. J. Yu, F. Zhu, J. Wang, A. C. Dunn, C. Zhou, Z. Xie, M. T. Agne, H. Wang, H. Luan, Y. Zhang, Y. Huang, G. J. Snyder and J. A. Rogers, *Sci. Adv.*, 2018, **4**, eaau5849-1243.
5. Q. Jin, S. Jiang, Y. Zhao, D. Wang, J. Qiu, D.-M. Tang, J. Tan, D.-M. Sun, P.-X. Hou, X.-Q. Chen, K. Tai, N. Gao, C. Liu, H.-M. Cheng and X. Jiang, *Nat. Mater.*, 2018, **3**, 10362.
6. G. Sebald, D. Guyomar and A. Agbossou, *Smart Mater. Struct.*, 2009, **18**, 125006.
7. M. S. Shur, A. D. Bykhovski and R. Gaska, *MRS Proc.*, 2011, **537**, G1.6.
8. Z. L. Wang and J. Song, *Science*, 2006, **312**, 242.
9. W. Wu, L. Wang, Y. Li, F. Zhang, L. Lin, S. Niu, D. Chenet, X. Zhang, Y. Hao, T. F. Heinz, J. Hone and Z. L. Wang, *Nature*, 2014, **514**, 470.
10. Z. L. Wang, *ACS Nano*, 2013, **7**, 9533-9557.
11. X. Huang, Y. Liu, G. W. Kong, J. H. Seo, Y. Ma, K.-I. Jang, J. A. Fan, S. Mao, Q. Chen, D. Li, H. Liu, C. Wang, D. Patnaik, L. Tian, G. A. Salvatore, X. Feng, Z. Ma, Y. Huang and J. A. Rogers, *Microsyst. Nanoeng.*, 2016, **2**, 16052.
12. X. Zhang, J. Grajal, J. L. Vazquez-Roy, U. Radhakrishna, X. Wang, W. Chern, L. Zhou, Y. Lin, P.-C. Shen, X. Ji, X. Ling, A. Zubair, Y. Zhang, H. Wang, M. Dubey, J. Kong, M. Dresselhaus and T. Palacios, *Nature*, 2019, **566**, 368-372.
13. A. Lorke, S. Wimmer, B. Jager, J. P. Kotthaus, W. Wegscheider and M. Bichler, *Physica B*, 1998, **249-251**, 312-316.
14. H. Linke, T. E. Humphrey, A. Löfgren, A. O. Sushkov, R. Newbury, R. P. Taylor and P. Omling, *Science*, 1999, **286**, 2314.
15. A. M. Song, P. Omling, L. Samuelson, W. Seifert, I. Shorubalko and H. Zirath, *Appl. Phys. Lett.*, 2001, **79**, 1357-1359.
16. E. M. Roeling, W. C. Germs, B. Smalbrugge, E. J. Geluk, T. de Vries, R. A. J. Janssen and M. Kemerink, *Nat. Mater.*, 2010, **10**, 51.
17. T. Tanaka, Y. Nakano and S. Kasai, *Jpn. J. Appl. Phys.*, 2013, **52**, 06GE07.
18. O. V. Mikhnenko, S. D. Collins and T.-Q. Nguyen, *Adv. Mater.*, 2015, **27**, 2007-2012.
19. O. Kedem, B. Lau, M. A. Ratner and E. A. Weiss, *Proc. Natl. Acad. Sci. USA*, 2017, **114**, 8698.
20. B. Lau, O. Kedem, M. Kodaimati, M. A. Ratner and E. A. Weiss, *Adv. Energy Mater.*, 2017, **7**, 1701000.
21. B. Lau and O. Kedem, *J. Chem. Phys.*, 2020, **152**, 200901.
22. P. Reimann, *Phys. Rep.*, 2002, **361**, 57-265.
23. P. Hänggi and F. Marchesoni, *Rev. Mod. Phys.*, 2009, **81**, 387-442.
24. H. Linke, W. D. Sheng, A. Svensson, A. Löfgren, L. Christensson, H. Q. Xu, P. Omling and P. E. Lindelof, *Phys. Rev. B*, 2000, **61**, 15914-15926.
25. Y. Abe, R. Kuroda, X. Ying, M. Sato, T. Tanaka and S. Kasai, *Jpn. J. Appl. Phys.*, 2015, **54**, 06FG02.
26. Y. Hu, V. Brus, W. Cao, K. Liao, H. Phan, M. Wang, K. Banerjee, G. C. Bazan and T.-Q. Nguyen, *Adv. Mater.*, 2017, **29**, 1606464.
27. K. Liao, S. D. Collins, V. V. Brus, O. V. Mikhnenko, Y. Hu, H. Phan and T.-Q. Nguyen, *ACS Appl. Mater. Interfaces*, 2019, **11**, 1081-1087.
28. J. Huang, A. Karki, V. V. Brus, Y. Hu, H. Phan, A. T. Lill, M. Wang, G. C. Bazan and T.-Q. Nguyen, *Adv. Mater.*, 2018, **30**, 1804794.
29. V. V. Brus, S. D. Collins, O. V. Mikhnenko, M. Wang, G. C. Bazan and T.-Q. Nguyen, *Adv. Electron. Mater.*, 2016, **2**, 1500344.
30. V. Coropceanu, J. Cornil, D. A. da Silva Filho, Y. Olivier, R. Silbey and J.-L. Brédas, *Chemical Reviews*, 2007, **107**, 926-952.
31. J. Zaumseil, *Adv. Electron. Mater.*, 2019, **5**, 1800514.

32. R. Ihly, K. S. Mistry, A. J. Ferguson, T. T. Clikeman, B. W. Larson, O. Reid, O. V. Boltalina, S. H. Strauss, G. Rumbles and J. L. Blackburn, *Nature Chemistry*, 2016, **8**, 603-609.
33. G. J. Brady, A. J. Way, N. S. Safron, H. T. Evensen, P. Gopalan and M. S. Arnold, *Sci. Adv.*, 2016, **2**, e1601240.
34. Y. Joo, G. J. Brady, C. Kanimozhi, J. Ko, M. J. Shea, M. T. Strand, M. S. Arnold and P. Gopalan, *ACS Appl. Mater. Interfaces*, 2017, DOI: 10.1021/acsami.7b06850, acsami.7b06850.
35. A. Chortos, C. Zhu, J. Y. Oh, I. Pochorovski, J. W. F. To, N. Liu, U. Kraft, B. Murmann and Z. Bao, *ACS Nano*, 2017, **11**, 7925-7937.
36. M. D. Bishop, G. Hills, T. Srimani, C. Lau, D. Murphy, S. Fuller, J. Humes, A. Ratkovich, M. Nelson and M. M. Shulaker, *Nat. Electron.*, 2020, **3**, 492-501.
37. J. L. Blackburn, S. D. Kang, M. J. Roos, B. Norton-Baker, E. M. Miller and A. J. Ferguson, *Adv. Electron. Mater.*, 2019, **2**, 1800910.
38. S. D. Collins, O. V. Mikhnenko, T. L. Nguyen, Z. D. Rengert, G. C. Bazan, H. Y. Woo and T.-Q. Nguyen, *Adv. Electron. Mater.*, 2017, **3**, 1700005.
39. C. Wang, L. Qian, W. Xu, S. Nie, W. Gu, J. Zhang, J. Zhao, J. Lin, Z. Chen and Z. Cui, *Nanoscale*, 2013, **5**, 4156-4161.
40. A. Chortos, I. Pochorovski, P. Lin, G. Pitner, X. Yan, T. Z. Gao, J. W. F. To, T. Lei, J. W. Will, H. S. P. Wong and Z. Bao, *ACS Nano*, 2017, **11**, 5660-5669.
41. L. S. C. Pingree, D. B. Rodovsky, D. C. Coffey, G. P. Bartholomew and D. S. Ginger, *J. Am. Chem. Soc.*, 2007, **129**, 15903-15910.
42. S. van Reenen, P. Matyba, A. Dzwilewski, R. A. J. Janssen, L. Edman and M. Kemerink, *J. Am. Chem. Soc.*, 2010, **132**, 13776-13781.
43. L. Bürgi, H. Sirringhaus and R. H. Friend, *Appl. Phys. Lett.*, 2002, **80**, 2913-2915.
44. L. Bürgi, T. J. Richards, R. H. Friend and H. Sirringhaus, *J. Appl. Phys.*, 2003, **94**, 6129-6137.
45. F. Chiarella, M. Barra, A. Carella, L. Parlato, E. Sarnelli and A. Cassinese, *Org. Electron.*, 2016, **28**, 299-305.
46. F. Chianese, F. Chiarella, M. Barra, A. Carella and A. Cassinese, *Org. Electron.*, 2018, **52**, 206-212.
47. J. C. deMello, N. Tessler, S. C. Graham and R. H. Friend, *Phys. Rev. B*, 1998, **57**, 12951-12963.
48. T. Minari, P. Darmawan, C. Liu, Y. Li, Y. Xu and K. Tsukagoshi, *Appl. Phys. Lett.*, 2012, **100**, 093303.
49. M. Waldrip, O. D. Jurchescu, D. J. Gundlach and E. G. Bittle, *Adv. Funct. Mater.*, 2020, **30**, 1904576.
50. X. Liu, C. Chen, L. Wei, N. Hu, C. Song, C. Liao, R. He, X. Dong, Y. Wang, Q. Liu and Y. Zhang, *Sci. Rep.*, 2016, **6**, 23319.

Broader Context

As portable electronic and sensing technologies, including wearable and implantable devices, become more prevalent there is a growing need to develop lightweight, flexible, and robust power sources that eliminate the need for battery storage. Electronic ratchet devices represent an emerging technology that could help to solve this growing problem, since they can harvest energy from unbiased external input signals with a zero time-average amplitude, such as background radio-frequency radiation. Despite impressive demonstrations of electronic ratchets based on organic semiconductors, there is still significant room to expand our understanding of the operating principles and to enhance their energy conversion performance. Here we show that doped carbon nanotube networks can be employed in electronic ratchets, exhibiting the highest power output reported to date for a simple device architecture. Our findings motivate further exploration of these materials and devices for portable power generation.